



Structural characterization of cellulose nanofibers isolated from spent coffee grounds and their composite films with poly(vinyl alcohol): a new non-wood source

Noriko Kanai · Takumi Honda · Naoki Yoshihara · Toshiyuki Oyama · Akira Naito · Kazuyoshi Ueda · Izuru Kawamura

Received: 21 August 2019 / Accepted: 19 March 2020 / Published online: 1 April 2020
© Springer Nature B.V. 2020

Abstract The waste valorization of spent coffee grounds (SCGs), which are obtainable in large amounts worldwide for new non-wood source has been considered. Cellulose nanofibers derived from SCGs have been successfully produced by 2,2,6,6-tetramethylpiperidine-1-oxyl radical (TEMPO)-mediated oxidation of SCGs containing 10% cellulose (dry weight). The TEMPO-oxidized cellulose nanofibers (TOCNFs) are 20–35 nm wide observed by scanning electron microscopy. X-ray diffraction showed that TOCNFs are present in a cellulose crystal form I. The average crystal size corresponding to a fiber width was 4.2 nm, as determined from the diffraction pattern. Solid-state NMR shows that hemicellulose and lignin were mostly removed from SCGs via TEMPO-

mediated oxidation, but small amounts of triacylglycerols remained in the TOCNFs. Thermogravimetric analysis of TOCNFs showed two major steps of thermal decomposition at 251 °C and 267 °C, which were higher than the coffee roasting temperature range. Furthermore, in order to investigate an interaction of these TOCNFs with a polymer, a SCG-derived TOCNF composite film with poly(vinyl alcohol) as a water-soluble polymer was prepared. We found the TOCNFs were successfully integrated into the polymer. The outcome of this study indicated that SCGs could be used as well as wood as an alternative source for producing TOCNFs, thus contributing to the development of sustainable green chemistry.

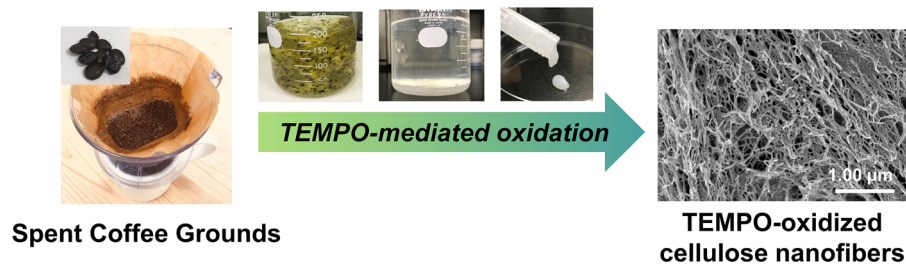
Electronic supplementary material The online version of this article (<https://doi.org/10.1007/s10570-020-03113-w>) contains supplementary material, which is available to authorized users.

N. Kanai · T. Oyama · I. Kawamura (✉)
Graduate School of Engineering Science, Yokohama National University, Yokohama, Japan
e-mail: izuruk@ynu.ac.jp

N. Yoshihara
Instrumental Analysis Center, Yokohama National University, Yokohama, Japan

T. Honda · T. Oyama · A. Naito · K. Ueda · I. Kawamura
Graduate School of Engineering, Yokohama National University, Yokohama, Japan

Graphic abstract



Keywords Cellulose nanofibers · Composite film · Poly(vinyl alcohol) · Spent coffee grounds · TEMPO-mediated oxidation · Waste revalorization

Introduction

More than nine million tons of coffee products were consumed worldwide in 2018 (International Coffee Organization 2019). At present, approximately six million tons of spent coffee grounds (SCGs) are generated annually worldwide (Mata et al. 2018). Approximately half of the overall SCGs are generated by the instant (i.e., soluble) coffee industry and major part of those SCGs are simply discarded or burned as fuel in the coffee industry (Cruz et al. 2012; Plaza et al. 2012). That results in the release of considerable amount of carbon dioxide and biologically toxic components, which pose environmental hazards (Atabani et al. 2019; Murthy and Naidu 2012; Mussatto et al. 2011b).

Over the last decade, research on SCGs aimed at waste revalorization has significantly increased, including novel approaches to reuse SCGs effectively in an eco-friendly manner (Campos-Vega et al. 2015; Obruca et al. 2015; Kovalcik et al. 2018). The valorization of SCGs have been proposed without any fractionation as substrates for the cultivation of microorganisms (Vítězová et al. 2019), lead removals from contaminated water (Lavecchia et al. 2016) and electrode materials (Wang et al. 2016). As low-cost raw material, bioactive components were extracted from SCGs, such as caffeine (Shang et al. 2017), chlorogenic acid (Ballesteros et al. 2017), kahweol and cafestol (Acevedo et al. 2013) for variety use in the food and pharmaceutical industries (Mata et al. 2018). In particular, extracting lipids containing

10–20% SCGs and its transformation into biodiesel oil has been demonstrated as a potential fuel feedstock (Atabani et al. 2019; Dang and Nguyen 2019; Karmee 2018; Kookos 2018; Jenkins et al. 2017). However, recycling SCG for the purposes mentioned above is still challenging due to its heterogeneity and economic inefficiency.

Almost half of the dry weight of SCGs consists of cellulose and hemicellulose, which can be exploited as sources of value-added materials (Arya and Rao 2007; Campos-Vega et al. 2015; Mussatto et al. 2011b). Cellulose constitutes approximately 10% of SCGs (Ballesteros et al. 2014; Mussatto et al. 2011a, b; Obruca et al. 2015). Extracting cellulose from SCGs requires extreme hydrolysis conditions such as lower pH, higher temperature, and reaction times (Mussatto et al. 2011b). This is caused by the fact that the coffee bean cell walls are formed with a strong honeycomb structure (Kanai et al. 2019; Kasai et al. 2006), making hydrolysis at mild conditions and the consequent cellulose extraction inefficient.

Native cellulose can be selectively isolated from plant cell walls by catalytic oxidation, using the 2,2,6,6-tetramethylpiperidine-1-oxyl radical (TEMPO) (Saito et al. 2007). When cellulose is oxidized with TEMPO, only hydroxyl groups on microfibril surface are converted to sodium carboxylate groups. These TEMPO-oxidized cellulose nanofibers (TOCNFs) can be transformed into discrete cellulose nanofibers (CNFs) with an average width of 3–5 nm by gently mechanical disintegration in water (Isogai et al. 2011; Isogai and Bergström 2018). The CNFs have been extracted not only from wood, but also from various non-wood materials including industrial residues, e.g., bamboo (Chen et al. 2017), cassava bagasse (Panyasiri et al. 2018), pineapple leaf (Balakrishnan et al. 2017), banana peel (Pelissari et al. 2014), oil palm (Rohaizu and Wanrosli 2017). The

number of non-wood CNF research publications constitutes more than 50% of the wood CNF publications in 2018 (Pennells et al. 2019); however, the preparation of CNFs from SCGs has not been reported yet.

In this study, we report SCGs as a completely new non-wood source of CNFs. SCG-derived TOCNFs have been produced and characterized using field emission scanning electron microscopy (FE-SEM), solid-state nuclear magnetic resonance spectroscopy (NMR), X-ray diffraction (XRD), and thermogravimetric analysis (TGA). We also present some preliminary results (SEM, solid-state NMR, TGA) for nanocomposite films of the SCG-derived TOCNFs with poly(vinyl alcohol) (PVA) as the matrix. In this paper, we presented SCGs have potential to be alternative source of wood-derived CNF as a view of structure of the TOCNF.

Materials and methods

Preparation of spent coffee grounds

Commercially available robusta roasted coffee beans (RCBs) from Indonesia and arabica RCBs from Tanzania were ground using an electric coffee grinder (Kalita, EG-45, Japan) for 70 s. Hot water was added to the ground RCBs. Wet-ground RCBs were spread thinly on filter paper and dried at room temperature for at least 1 day. Completely dried ground RCBs were termed SCGs. Triacylglycerol (TAG), the main lipid present in SCGs, was removed by stirring in *n*-hexane for 2 days (Kanai et al. 2019). After delipidation, SCGs were termed solid residues. As a comparative sample, microcrystalline cellulose (MCC, 20 µm wide) was purchased from Sigma-Aldrich.

TEMPO-mediated oxidation

Solid residues (1 g) were suspended in distilled water (130 mL) containing TEMPO (20 mg, 98%, Sigma-Aldrich) and NaBr (0.1 g, ≥ 99.0%, Sigma-Aldrich). TEMPO-mediated oxidation was initiated with the addition of NaClO (60 mL, 3–5%, Sigma-Aldrich) at pH 10–10.5 and room temperature. The TEMPO-mediated oxidation was performed for 3 h upon continuous stirring, and the pH was kept at 10–10.5 by adding 0.5 M NaOH or 1 M HCl during oxidation.

The end of the oxidation reaction was detected when pH did not change for 10 min (Isogai 2018). Ethanol (10 mL) was added to quench TEMPO-mediated oxidation. The oxidized cellulose was filtered out under vacuum (filter paper with 3.0 µm pores) and then washed 3 times with distilled water. An aliquot of the collected cellulose slurry was lyophilized with a freeze-dryer (EYELA, FDU-2100) for 2 days to determine its dry mass. The cellulose slurry was dispersed to 1.5 wt% in distilled water and sonicated for 2–3 min with a homogenizer (BRANSON, Sonifier Analog Series 250) using the setting of output:3 and duty cycle:41% to obtain a gel-like TOCNF dispersion.

Preparation of composite films

PVA (polymerization degree approximately 1500, saponification degree 86.0–90.0 mol%, Wako Pure Chemicals Co., Japan) powder was dissolved (1.0 M) into distilled water for 10 min, and subsequently stirred at 90 °C for 1 h. After cooling to room temperature, 1.0 M PVA solution was added to a TOCNF dispersion (1.5 wt%) at 50 wt% loading and stirred for 3 days. PVA/TOCNF dispersion was then carefully and uniformly cast into a Teflon square dish and dried with a constant temperature dryer (DRV320DE, Advantec Tokyo Co., Ltd., Japan) at 40 °C overnight in vacuo.

SEM

The gel-like TOCNF dispersion (0.5 g) was washed with *tert*-butanol (10 mL, ≥ 99.0%, Sigma-Aldrich). The dispersion was centrifuged at 15,000g for 5 min (MX-305, Suprema 21, TOMY), and the supernatant was removed. This process was repeated 10 times, replacing solvent; after that, the TOCNFs were lyophilized for 6 days. The completely dried TOCNF powder was observed on a field emission scanning electron microscopy (FE-SEM) (HITACHI, SU8010) coated with osmium at 1.0 kV (Fig. 1a) and with Pt–Pd at 0.5 kV (Fig. 1b). PVA/TOCNF composite films covered with Pt–Pd coating were also observed on FE-SEM, with an accelerating voltage of 1.0 kV.

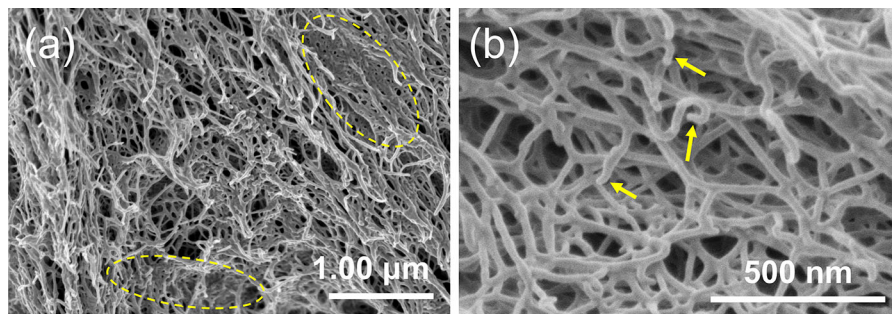


Fig. 1 SEM images of SCG-derived TOCNFs differing in scale bars: **a** 1.00 μm and **b** 500 nm

Solid-state NMR

The solid materials such as TOCNF powder, PVA film, and PVA/TOCNF composite films were directly packed into a 4.0 mm outer diameter zirconia rotor. ^{13}C cross-polarization magic angle spinning (CP-MAS) solid-state NMR spectra were recorded on a 600 MHz NMR spectrometer (Bruker Avance III) equipped with a 4.0 mm ^1H – ^{13}C – ^{15}N triple resonance E-free MAS probe at room temperature with a contact time of 1.0 ms and a recycle delay time of 3 s. MAS frequencies were 13, 10 and 12.5 kHz for TOCNF powder, MCC samples, and composite films, respectively. ^{13}C chemical shifts were externally referenced to tetramethylsilane (0.0 ppm). The NMR measurements were operated in TOPSPIN software as well as the data processing and peak deconvolution.

XRD

XRD experiments were performed using an X-ray diffractometer operating at 40 kV and 45 mA at room temperature. The hydrated sample was placed on a non-reflective sample plate and was dried for 3 h using vacuum dryer. The powder-XRD patterns were recorded with Cu $K\alpha$ radiation ($\lambda = 0.15418$ nm) at a step size of 0.05° over the 5° – 50° 2θ range with a scanning speed of $0.3^\circ/\text{min}$. The patterns were corrected using a blank and then analyzed using the pseudo-Voigt function for peak deconvolution (Ling et al. 2019).

TGA

TGA was performed to compare the stability of TOCNFs and MCC. Approximately 1 mg of each

sample was placed in an aluminum pan, using an empty pan as a reference. TGA was performed using an STA 2500 Regulus (NETZSCH Co., Ltd, Germany) at a temperature range of 30 – 450 $^\circ\text{C}$ with an increasing temperature rate of 10.0 $^\circ\text{C}/\text{min}$ under a helium stream with a flow rate of 50.0 mL/min. The neat PVA and the composite PVA/TOCNF films were also measured by a TGA-50 (Shimadzu Co., Ltd, Japan) using a platinum cell from 25 to 800 $^\circ\text{C}$ with an increase of 10.0 $^\circ\text{C}/\text{min}$, under a nitrogen gas stream at a flow rate of 50.0 mL/min. The derivative thermogravimetric data of the films were smoothed with a 50-point adjacent averaging smooth function.

Results

Characterization of SCG-derived TOCNFs

SEM images of TOCNFs prepared from SCGs are shown in Fig. 1. As shown in Fig. 1a, TOCNFs are susceptible to partial aggregation during the drying process, which makes it difficult to distinguish the borders of TOCNF; however, most TOCNFs are well separated from each other (Fig. 1b). The termination of TOCNFs tends to be bent as shown in Fig. 1b. The diameters of SCG-derived TOCNFs were found to be in a range of 20 – 35 nm with an average diameter of 25 nm ($n = 30$, n : the number of TOCNFs to calculate the average diameter).

To characterize the final material, we performed ^{13}C solid-state NMR experiments. The signals at 60 – 110 ppm correspond to glucose units in cellulose (Fig. 2). Namely, the C6 (62.8 and 65.3 ppm), C2, C3, C5 (72.4 and 75.0 ppm), C4 (83.9 and 89.1 ppm), and C1 (105.3 ppm) groups were assigned.

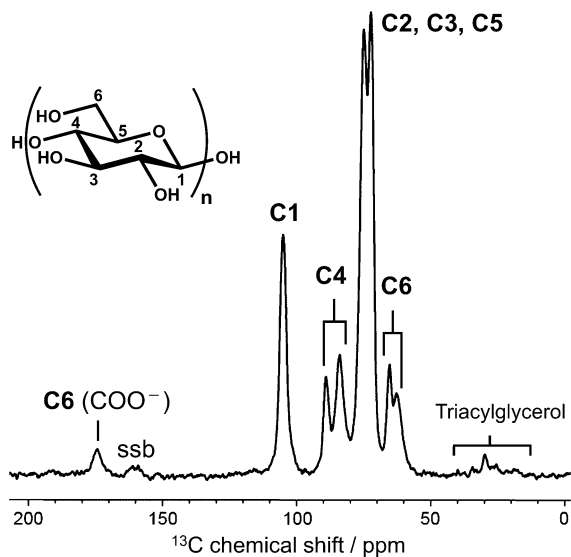


Fig. 2 ^{13}C CP-MAS NMR spectrum of SCG-derived TOCNFs with signal assignment. “ssb” represents spinning sidebands. The chemical structure of cellulose is shown on the upper left

Hemicelluloses, which mainly contain mannose, galactose, and arabinose, and lignin signals did not appear in the ^{13}C NMR spectrum (Fu et al. 2015; Mussatto et al. 2011b; Liitiä et al. 2003); however, traces of TAG appeared at 20–35 ppm (Kanai et al. 2019). The lower field isolated peak at 174.2 ppm was assigned to a carboxylic acid (COO^-), indicating the successful TEMPO-mediated oxidation of SCGs (Saito et al. 2007). Furthermore, the ^{13}C chemical shifts of C4 and C6 carbons are highly sensitive to the cellulose crystal structure and hence, the crystallinity of the TOCNFs could be determined by comparing the separated areas (Saito et al. 2005). The C4 of the TOCNFs resonated at 89.1 ppm for the crystalline state, and 83.9 ppm for the non-crystalline (or amorphous) state (Park et al. 2010). The crystallinity of TOCNFs was estimated to be 32% by deconvolution analysis of the C4 NMR signal, which is 16% lower than that of MCC (supporting Figure S2).

The powder-XRD pattern was recorded in order to determine the crystal structure and degree of crystallinity of the SCG-derived TOCNFs (Fig. 3). The XRD patterns showed typical cellulose I as expected, with two distinct crystal phases $\text{I}\alpha$ and $\text{I}\beta$ in various proportions (Nishiyama et al. 2002; Poletto et al. 2013). The three main peaks at 14.9° , 16.7° , and 22.6° for cellulose $\text{I}\beta$ were assigned to Miller indices of (1-10), (110), and (200), respectively, which are the

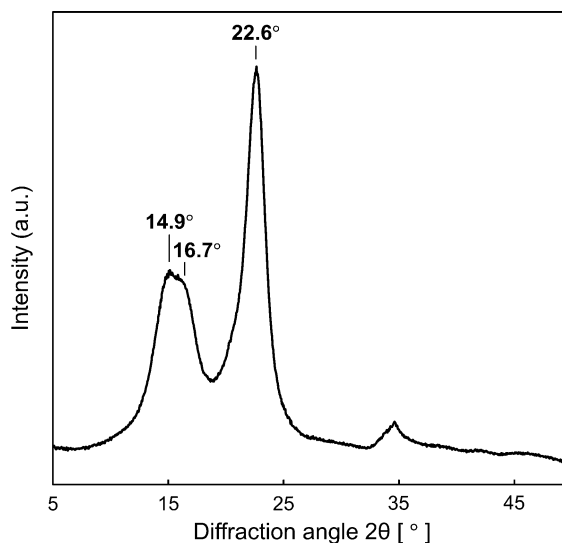


Fig. 3 Powder-XRD pattern of SCG-derived TOCNFs (a.u., arbitrary unit) measured at room temperature

counterparts to the (100), (010), and (110) peaks of the cellulose $\text{I}\alpha$ pattern (French 2014). The average crystal size corresponding to fiber width of the TOCNF was 4.2 nm, as calculated from the (22.6°) diffraction peak using the Scherrer equation (Scherrer 1918). The shape factor, i.e., K was taken as 0.9. Furthermore, it was possible to evaluate the sample crystallinity by deconvolution of the XRD pattern (Ling et al. 2019; Park et al. 2010). The crystallinity of the TOCNF (72%) was slightly lower than MCC (79%) (Supporting Figures S3 and S4), which was consistent with the trend calculated from NMR deconvolution analysis of the C4 signal.

As shown by the solid black line in Fig. 4, the TOCNF started to degrade earlier than MCC. The TOCNF showed gradual weight loss due to the strongly bounded water beginning at around 100°C . Then, overlapping degradation occurred within 150°C and 250°C due to decarboxylation of the sodium carboxylate groups and dehydration of the cellulose chains (Lichtenstein and Lavoine 2017). The major degradation process of the TOCNF occurred in two steps at 251°C and 267°C . In the first step, sodium hydro-glucuronate units were decomposed and in the second step, unaltered cellulose units were decomposed (Fukuzumi et al. 2010). The second degradation temperature is 77°C lower than maximum weight loss of MCC. This indicates that crystalline cellulose chains decrease in peak points

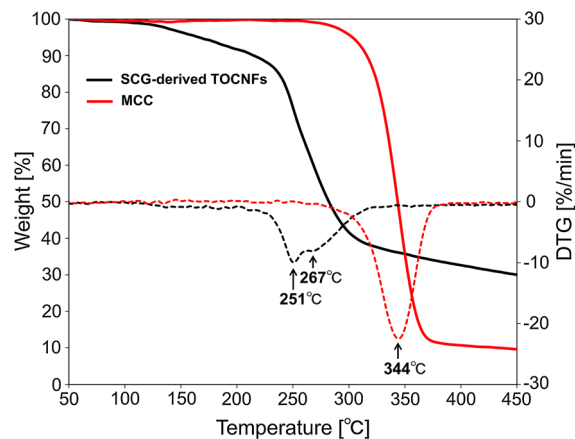


Fig. 4 Thermogravimetric curves of SCG-derived TOCNFs (solid black line) and MCC (solid red line), and derivative thermogravimetric curves (SCG-derived TOCNFs: dashed black line, MCC: dashed red line). Thermal degradation temperature of each sample is shown in DTG curves

due to thermally unstable anhydroglucuronate units in the TOCNF (Cao et al. 2012). Compared to MCC, the TOCNF showed much higher char residues (30 wt%) at 450 °C. According to Lichtenstein and Lavoine (2017), sodium cation as a counterion influenced the char production.

Preparation and structure characterization of PVA/TOCNF composite film

In order to investigate an interaction of the TOCNF with PVA polymer, structure of composite film was characterized by solid-state NMR and TG/DTA. A transparent composite film of 1:1 PVA/TOCNF was prepared, and it became slightly yellowish during a drying procedure (Figure S5). Morphology of the PVA/TOCNF composite film was observed by SEM as shown in Fig. 5. The surface of the film confirmed a

high degree of uniformity, although air bubbles were observed when water was evaporated (Fig. 5a). TOCNFs aggregated in the film during the drying process and appeared as sharp tips in the cross-sections (Fig. 5b).

In the ^{13}C solid-state NMR spectrum of PVA/TOCNF (1:1), the TOCNF and PVA signals were unambiguously observed (Fig. 6). The identifiable C1, C4 and carbonyl signals corresponding to TOCNF in the composite film were slightly shifted compared to that of the TOCNFs itself (the TOCNF in the composite film/the SCG-TOCNF; C1 104.8/105.3 ppm, C4 88.9/89.1 and 83.9/83.9 ppm, carbonyl 173.3/174.2 ppm). Especially, the carbonyl carbon of the TOCNF, which appeared originally at 174.2 ppm, slightly higher-field shift to 173.3 ppm on blending with the PVA polymer. The systematic NMR peak shifts of carbonyl carbon signals in cellulose acetate/VP-MMA polymer indicated that the blending with the VP-MMA copolymer disrupted intra- and inter-hydrogen bonding in the original cellulose acetate itself (Ohno and Nishio 2007). Therefore, our NMR result of the composite film is suggested that the blending with PVA polymer altered the hydrogen bonding behavior of the TOCNF, resulting the presence of interaction of the TOCNF with the water-soluble polymer. The signals at 60–80 ppm and 36–51 ppm have been assigned to the methine and methylene groups in PVA, respectively. Hydrogen bonding in the PVA film broadened the CH signal significantly (Kobayashi et al. 1998; Masuda et al. 2000). The low-intensity peak at 30 ppm corresponds to the remaining TAG. The saponification degree of PVA was 86.0–90.0 mol%, and therefore signals derived from polyvinyl acetate (PVAc, Scheme S1

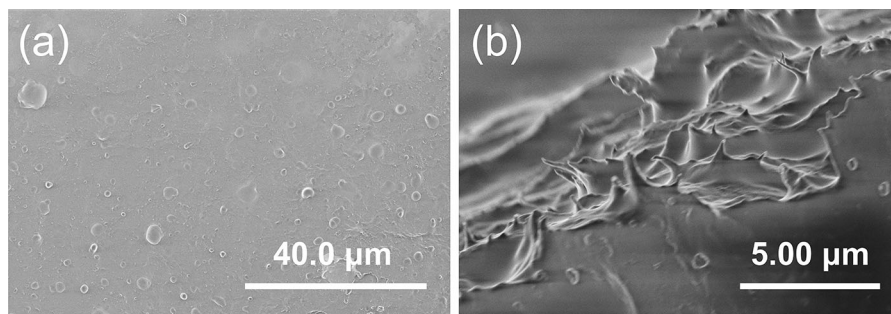


Fig. 5 SEM images of a PVA/TOCNF (1:1) transparent composite film: **a** on surface and **b** in cross-sections

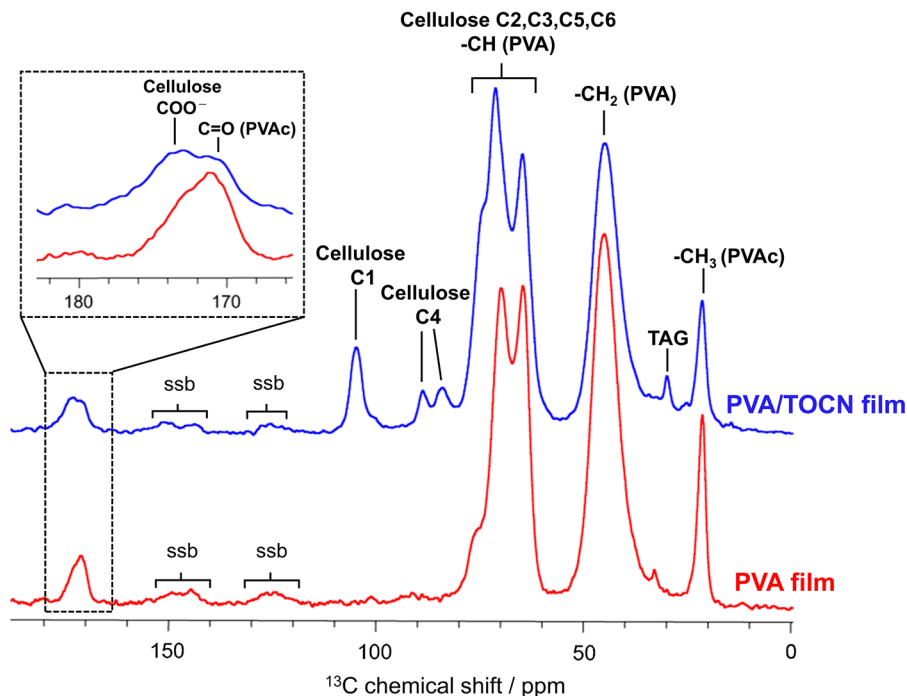


Fig. 6 ^{13}C solid-state NMR spectra of PVA/TOCNF (blue) and PVA (red) films. ssb: spinning sidebands

in the Supporting Information) appeared at 21.4 ppm and 171.2 ppm in both spectra (Comotti et al. 1997).

The TGA and corresponding DTG curves of TOCNF, PVA/TOCNF, and PVA films are shown in Fig. 7. There is an initial weight loss of up to 8% for all the three samples at around 100 °C corresponding to absorbed moisture in the films (Fukuzumi et al. 2009;

Lee et al. 2009). Neat TOCNF and PVA films were found to show maximum weight loss at 255 °C (Fig. 7b t_1) and 313 °C (Fig. 7b p_1), respectively, as extracted from the corresponding DTG curves. In the case of PVA/TOCNF composite film, the decomposition temperature was recorded at about 289 °C which lies between those of the respective single films

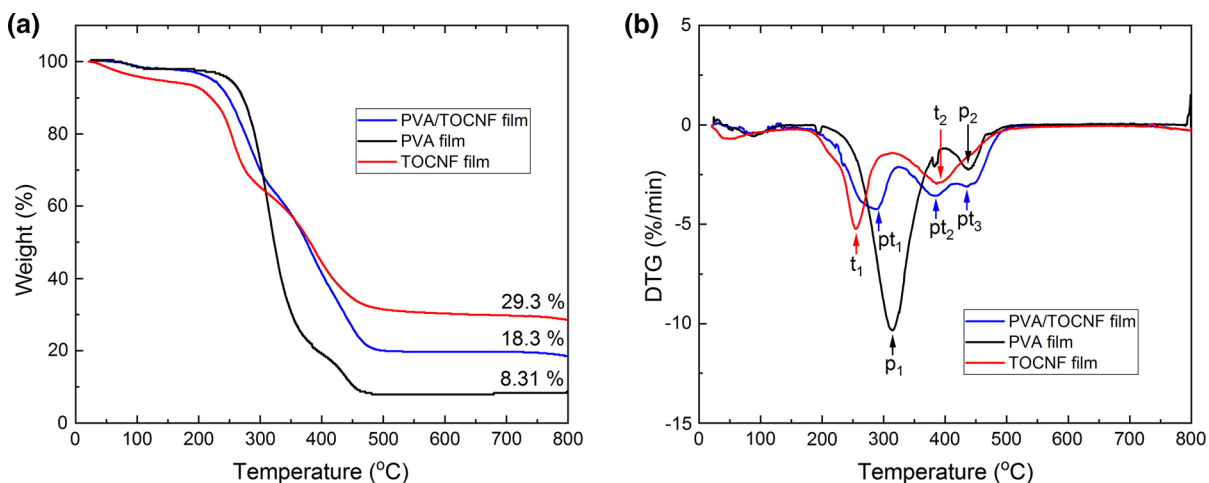


Fig. 7 **a** Thermogravimetric (TG) and **b** derivative thermogravimetric (DTG) curves of PVA/TOCNF (blue), PVA (black) and TOCNF (red) films

(Fig. 7b pt₁). This result confirms that TOCNFs were successfully integrated into the PVA, most probably via hydrogen bonding between hydroxyl groups in TOCNFs and PVA. On the other hand, the weight loss occurred at around 380 °C in the neat TOCNF (Fig. 7b t₂) and 435 °C in the neat PVA (Fig. 7b p₂) films showed a similar temperature to those two corresponding degradations in the PVA/TOCNF composite film (Fig. 7b pt₂ and pt₃). Those two steps were probably due to each respective decomposition of PVA and cellulose structure in the films or carbonaceous matter (Lee et al. 2009).

Discussion

Cellulose microfibrils vary widely in size, from 2 to 30 nm, depending on the cellulose source (Börjesson and Westman 2015). As an example, the completely individualized microfibril obtained from wood is 3–4 nm wide, which is the smallest elements next to cellulose molecules consisting of 30–40 cellulose chains (Isogai et al. 2011). The average diameter of SCG-derived TOCNFs was 25 nm, as shown in Fig. 1, suggesting that a few microfibril units are still fibrillated in the average crystal size revealed from the powder-XRD pattern. The most likely reason for insufficient fibrillation is quite high ratio of hemicelluloses (30–40 wt%), lignin (19.8–29.8 wt%) and TAG in SCGs (Kovalcik et al. 2018). Remaining TAG revealed in the ¹³C CP-MAS NMR spectrum (Fig. 2) may prevent complete disconnection. Also, there is a possibility that unobservable small amounts of hemicelluloses and lignin in NMR spectrum remain in TOCNFs. According to Isogai et al. (2011), hemicelluloses and lignin can be removed as water-soluble degraded fractions in TEMPO/NaBr/NaClO oxidation system. In this study, the required amount of NaClO in the TEMPO system was 3–18 times higher than holocelluloses reported by Kuramae et al. (2014). This suggests that plenty of NaClO was consumed in solubilization of hemicelluloses and lignin. The most beneficial feature of using TEMPO is to be able to get 3–4 nm narrow fibers. In order to achieve nanofibrillation into the completely individualized microfibril, some pre-treatment with mild alkali and sodium chlorite for removing hemicelluloses and lignin to some extent is considered to be needed (Wise et al. 1946).

Another crucial structural feature estimated from chemical shifts in the ¹³C NMR spectrum (Fig. 2) is the conformation of CH₂OH (C6–OH) in cellulose. There are three possible conformations that can be distinguished. The C6 signal is sensitive to this conformational change and can be considered as a diagnostic region; *gauche-gauche* (*gg*, 60–62.6 ppm), *gauche-trans* (*gt*, 62.5–64.5 ppm), and *trans-gauche* (*tg*, 65.5–66.5 ppm) (Horii et al. 1983). In our case, the signal at 65.3 ppm corresponding to C6 can indicate the presence of the *tg* conformer. Native cellulose predominantly displays the *tg* conformation inside microfibrils, allowing the formation of intramolecular hydrogen bonds between O3 and O5, and O6 and O2 (Miyamoto et al. 2013; Nishiyama et al. 2002). On the other hand, the amorphous C6 peak at 62.8 ppm reflects the structure of the surface cellulose chains and may have both *gt* and *gg* conformations (Phyo et al. 2018; Yang et al. 2018).

The different crystallinity of the TOCNFs were estimated by XRD and NMR analysis (72% and 32%). There are several reasons for significant differences in crystallinity index can be observed depending on whether XRD peak or ¹³C NMR peak deconvolutions is used (Ioelovich 2016). Firstly, the results from the former method usually generate higher values than the latter, because of differences in measurement principles and analysis techniques (Park et al. 2009, 2010). Secondly, the XRD crystallinity index of textured sample has a tendency to be higher than that of non-textured sample (Ioelovich 2016, Rongpipi et al. 2019). Thus, the density and thickness of our XRD sample might influence the index. Thirdly, adding of signals of paracrystalline layers of crystalline and amorphous domains in C4 NMR peak deconvolution leads to decrease of a crystalline index value (Ioelovich 2016). It is previously suggested that there is a paracrystalline region in cellulose, which is less ordered with a somewhat larger mobility than the crystalline cellulose structure (Larsson et al. 1997). The surface induced by fibril aggregation is often presented as a disordered form with a very broad component around 84 ppm. However, the observed C4 signal at 83.9 ppm of SCGs-derived TOCNFs was not so much broad than that of crystalline component at 89.1 ppm (Fig. 2). By dynamic nuclear polarization (DNP) NMR experiments, well-resolved narrow C4 NMR signals of ball-milled cotton cellulose around 84 ppm suggested partial order component has been

identified in the disordered domains (Ling et al. 2019; Kirui et al. 2019). Therefore, above reasons can be assumed that the difference of the crystallinity index of the TOCNFs. Importantly, the ^{13}C NMR method is reasonable to use with lignin-removed cellulose samples (Daicho et al. 2018). As compared with ^{13}C CP-MAS NMR spectra of RCBs and hexane-treated coffee residues (Kanai et al. 2019), our SCG-derived TOCNFs did not contain mostly lignin and hemicellulose as mentioned above.

The average crystal size of the TOCNFs (4.2 nm) from XRD is ~ 1 nm larger than that of other non-wood resources but relatively close to that of TEMPO-oxidized cellulose from softwood (3.8 nm) and hardwood (3.8 nm) (Kuramae et al. 2014; Okita et al. 2010; Puangsin et al. 2013). This demonstrates that SCG-derived TOCNFs show similar characteristics as wood-based TOCNFs. In addition, further investigation to generate completely individualized TOCN is warranted.

Inserting sodium carboxylate groups via TEMPO-mediated oxidation resulted in a significant decrease in temperature of thermal degradation; however, our results are within the temperature range of wood-based materials (Fukuzumi et al. 2009), indicating that the thermal stability of SCG-derived TOCNFs may be comparable to that of wood-derived TOCNFs. The roasting temperature of coffee beans is generally in the range of 170–230 °C for 10–15 min (Illy and Viani 1995); therefore, the celluloses contained in coffee beans and the resulting SCGs are not degraded during the roasting process.

PVA was chosen as a versatile matrix because of its film-forming ability as well as biocompatibility for TOCNFs (Yang et al. 2008; Khalil et al. 2014). Further investigation of composite materials based on SCG-derived TOCNFs will need to be performed but these preliminary results indicate compatibility.

Conclusions

This is a detailed structural study report of cellulose nanofibers derived from SCGs as a promising new non-wood source of CNFs. We have shown that TEMPO-mediated oxidation can be used to produce CNFs from SCGs without pre-processing steps of crushing. Purified SCG-derived TOCNFs were defined fibers in the width of 25 nm. In ^{13}C CP-

MAS NMR spectrum of SCGs-derived TOCNFs, the isolated carbonyl peak appeared, indicating the successful TEMPO-mediated oxidation to the cellulose in SCGs. The XRD analysis revealed the crystal structure of the TOCNFs is present in a typical polymorphic cellulose I form. The TOCNFs showed a characteristic thermal decomposition behavior by the TEMPO-mediated oxidation. Namely, structure and thermal property of the SCG-derived TOCNFs is similar to wood-derived TOCNFs.

Further, using the SCGs-derived TOCNFs, the composite film with PVA polymer was prepared. Solid-state NMR and TG/DTG experiments of the film revealed that the TOCNFs were sufficiently integrated with the PVA polymer. Thus, the SCGs-derived TOCNFs provides a possibility of compatibility to forming the composite film.

Acknowledgments We thank Prof. Akira Isogai and Dr. Yuko Ono from the University of Tokyo for their helpful advice regarding TEMPO-mediated oxidation and structural characterization. We thank Prof. Atsumi Miyake from the Institute of Advanced Sciences, Yokohama National University and Dr. Yu-ichiro Izato and Ms. Nana Yamaki from Graduate School of Environment and Information Sciences, Yokohama National University for their technical assistance with the optimization of the TGA. We thank Dr. Eliška Procházková from the Czech Academy of Sciences for proof-reading the manuscript.

Funding This work was financially supported by “YNU Diversity Research Grant” under MEXT Funds for the Development of Human Resources in Science and Technology, “Initiative for Realizing Diversity in the Research Environment (Collaboration Type)” and the ROUTE (Research Opportunity for Undergraduates) program from Yokohama National University to N. K., and the Japan Society for the Promotion of Science (JSPS) KAKENHI Grant in Scientific Research (B) (JP18H02387) and Yokohama Academic Foundation (674) to I. K.

Compliance with ethical standards

Conflict of interest The authors declare no conflict of interest.

References

- Acevedo F, Rubilar M, Scheuermann E, Cancino B, Uquiche E, Garcés M, Inostroza K, Shene C (2013) Spent coffee grounds as a renewable source of bioactive compounds. *J Biobased Mater* 7:420–428. <https://doi.org/10.1166/jbmb.2013.1369>

- Arya M, Rao LJM (2007) An impression of coffee carbohydrates. *Crit Rev Food Sci Nutr* 47:51–67. <https://doi.org/10.1080/10408390600550315>
- Atabani AE, Al-Muhtaseb AH, Kumar G, Saratale GD, Aslam M, Khan HA, Said Z, Mahmoud E (2019) Valorization of spent coffee grounds into biofuels and value-added products: pathway towards integrated bio-refinery. *Fuel* 254:115640. <https://doi.org/10.1016/j.fuel.2019.115640>
- Balakrishnan P, Sreekala MS, Kunaver M, Huskić M, Thomas S (2017) Morphology, transport characteristics and viscoelastic polymer chain confinement in nanocomposites based on thermoplastic potato starch and cellulose nanofibers from pineapple leaf. *Carbohydr Polym* 169:176–188. <https://doi.org/10.1016/j.carbpol.2017.04.017>
- Ballesteros LF, Teixeira JA, Mussatto SI (2014) Chemical, functional, and structural properties of spent coffee grounds and coffee silverskin. *Food Bioprocess Technol* 7:3493–3503. <https://doi.org/10.1007/s11947-014-1349-z>
- Ballesteros LF, Ramirez MJ, Orrego CE, Teixeira JA, Mussatto SI (2017) Optimization of autohydrolysis conditions to extract antioxidant phenolic compounds from spent coffee grounds. *J Food Eng* 199:1–8. <https://doi.org/10.1016/j.jfoodeng.2016.11.014>
- Börjesson M, Westman G (2015) Crystalline nanocellulose—preparation, modification, and properties. In: *Cellulose—fundamental aspects and current trends*. Intech, pp 159–191
- Campos-Vega R, Loarca-Piña G, Vergara-Castañeda HA, Oomah BD (2015) Spent coffee grounds: a review on current research and future prospects. *Trends Food Sci Technol* 45:24–36. <https://doi.org/10.1016/j.tifs.2015.04.012>
- Cao X, Ding B, Yu J, Al-Deyab SS (2012) Cellulose nanowhiskers extracted from TEMPO-oxidized jute fibers. *Carbohydr Polym* 90:1075–1080. <https://doi.org/10.1016/j.carbpol.2012.06.046>
- Chen Y, Geng B, Ru J, Tong C, Liu H, Chen J (2017) Comparative characteristics of TEMPO-oxidized cellulose nanofibers and resulting nanopapers from bamboo, softwood, and hardwood pulps. *Cellulose* 24:4831–4844. <https://doi.org/10.1007/s10570-017-1478-4>
- Comotti A, Simonutti R, Sozzani P (1997) Morphology of the poly(vinyl alcohol)-poly(vinyl acetate) copolymer in microdefect-free composites: a ^{13}C magic-angle-spinning nuclear magnetic resonance and ^1H spin-diffusion study. *J Mater Sci* 32:4237–4245. <https://doi.org/10.1023/A:1018695000769>
- Cruz R, Cardoso MM, Fernandes L, Oliveira M, Mendes E, Baptista P, Morais S, Casal S (2012) Espresso coffee residues: a valuable source of unextracted compounds. *J Agric Food Chem* 60:7777–7784. <https://doi.org/10.1021/jf3018854>
- Daicho K, Saito T, Fujisawa S, Isogai A (2018) The crystallinity of nanocellulose: dispersion-induced disordering of the grain boundary in biologically structured cellulose. *ACS Appl Nano Mater* 1:5774–5785. <https://doi.org/10.1021/acsnm.8b01438>
- Dang CH, Nguyen TD (2019) Physicochemical characterization of *robusta* spent coffee ground oil for biodiesel manufacturing. *Waste Biomass Valori* 10:2703–2712. <https://doi.org/10.1007/s12649-018-0287-9>
- French AD (2014) Idealized powder diffraction patterns for cellulose polymorphs. *Cellulose* 21:885–896. <https://doi.org/10.1007/s10570-013-0030-4>
- Fu L, McCallum SA, Miao J, Hart C, Tudryn GJ, Zhang F, Linhardt RJ (2015) Rapid and accurate determination of the lignin content of lignocellulosic biomass by solid-state NMR. *Fuel* 141:39–45. <https://doi.org/10.1016/j.fuel.2014.10.039>
- Fukuzumi H, Saito T, Iwata T, Kumamoto Y, Isogai A (2009) Transparent and high gas barrier films of cellulose nanofibers prepared by TEMPO-mediated oxidation. *Biomacromolecules* 10:162–165. <https://doi.org/10.1021/bm801065u>
- Fukuzumi H, Saito T, Okita Y, Isogai A (2010) Thermal stabilization of TEMPO-oxidized cellulose. *Polym Degrad Stab* 95:1502–1508. <https://doi.org/10.1016/j.polymdegradstab.2010.06.015>
- Horii F, Hirai A, Kitamaru R (1983) Solid-state ^{13}C -NMR study of conformations of oligosaccharides and cellulose. *Polym Bull* 10:357–361. <https://doi.org/10.1007/BF00281948>
- Illy A, Viani R (1995) Espresso coffee, the chemistry of quality. Academic, London, p 198
- International Coffee Organization (2019) World coffee consumption. <http://www.ico.org/prices/new-consumption-table.pdf>. Accessed 3rd Feb 2020
- Ioelovich M (2016) Physicochemical methods for determination of cellulose crystallinity. *ChemXPress* 9:245–251
- Isogai A (2018) Development of completely dispersed cellulose nanofibers. *Proc Jpn Acad Ser B Phys Biol Sci* 94:161–179. <https://doi.org/10.2183/pjab.94.012>
- Isogai A, Bergström L (2018) Preparation of cellulose nanofibers using green and sustainable chemistry. *Curr Opin Green Sustain Chem* 12:15–21. <https://doi.org/10.1016/j.cogsc.2018.04.008>
- Isogai A, Saito T, Fukuzumi H (2011) TEMPO-oxidized cellulose nanofibers. *Nanoscale* 3:71–85. <https://doi.org/10.1039/c0nr00583e>
- Jenkins RW, Ellis EH, Lewis EJ, Paterson M, Le CD, Ting VP, Chuck CJ (2017) Production of biodiesel from vietnamese waste coffee beans: biofuel yield, saturation and stability are all elevated compared with conventional coffee biodiesel. *Waste Biomass Valoriz* 8:1237–1245. <https://doi.org/10.1007/s12649-016-9715-x>
- Kanai N, Yoshihara N, Kawamura I (2019) Solid-state NMR characterization of triacylglycerol and polysaccharides in coffee beans. *Biosci Biotechnol Biochem* 83:803–809. <https://doi.org/10.1080/09168451.2019.1571899>
- Karmee SK (2018) A spent coffee grounds based biorefinery for the production of biofuels, biopolymers, antioxidants and biocomposites. *Waste Manag* 72:240–254. <https://doi.org/10.1016/j.wasman.2017.10.042>
- Kasai N, Konishi A, Iwai K, Maeda G (2006) Efficient digestion and structural characteristics of cell walls of coffee beans. *J Agric Food Chem* 54:6336–6342. <https://doi.org/10.1021/jf0609072>
- Khalil HPSA, Davoudpour Y, Islam MN, Mustapha A, Sudesh K, Dungani R, Jawaid M (2014) Production and modification of nanofibrillated cellulose using various mechanical processes: a review. *Carbohydr Polym* 99:649–665. <https://doi.org/10.1016/j.carbpol.2013.08.069>

- Kirui A, Ling Z, Kang X, Widanage MCD, Mentink-Vigier F, French AD, Wang T (2019) Atomic resolution of cotton cellulose structure enabled by dynamic nuclear polarization solid-state NMR. *Cellulose* 26:329–339. <https://doi.org/10.1007/s10570-018-2095-6>
- Kobayashi M, Ando I, Ishii T, Amiya S (1998) Structural and dynamical studies of poly(vinyl alcohol) gels by high-resolution solid-state ^{13}C NMR spectroscopy. *J Mol Struct* 440:155–164. [https://doi.org/10.1016/S0022-2860\(97\)00238-X](https://doi.org/10.1016/S0022-2860(97)00238-X)
- Kookos IK (2018) Technoeconomic and environmental assessment of a process for biodiesel production from spent coffee grounds (SCGs). *Resour Conserv Recycl* 134:156–164. <https://doi.org/10.1016/j.resconrec.2018.02.002>
- Kovalcik A, Obruca S, Marova I (2018) Valorization of spent coffee grounds: a review. *Food Bioprod Process* 110:104–119. <https://doi.org/10.1016/j.fbp.2018.05.002>
- Kuramae R, Saito T, Isogai A (2014) TEMPO-oxidized cellulose nanofibrils prepared from various plant holocelluloses. *React Funct Polym* 85:126–133. <https://doi.org/10.1016/j.reactfunctpolym.2014.06.011>
- Larsson PT, Wickholm K, Iversen T (1997) A CP/MAS ^{13}C NMR investigation of molecular ordering in celluloses. *Carbohydr Res* 302:19–25. [https://doi.org/10.1016/S0008-6215\(97\)00130-4](https://doi.org/10.1016/S0008-6215(97)00130-4)
- Lavecchia R, Medici F, Patterer MS, Zuorro A (2016) Lead removal from water by adsorption on spent coffee grounds. *Chem Eng Trans* 47:295–300. <https://doi.org/10.3303/CET1647050>
- Lee SY, Mohan DJ, Kang IA, Doh GH, Lee S, Han SO (2009) Nanocellulose reinforced PVA composite films: effect of acid treatment and filler loading. *Fibers Polym* 10:77–82. <https://doi.org/10.1007/s12221-009-0077-x>
- Lichtenstein K, Lavoine N (2017) Toward a deeper understanding of the thermal degradation mechanism of nanocellulose. *Polym Degrad Stab* 146:53–60. <https://doi.org/10.1016/j.polymdegradstab.2017.09.018>
- Liitiä T, Maunu SL, Hortling B, Tamminen T, Pekkala O, Varhimo A (2003) Cellulose crystallinity and ordering of hemicelluloses in pine and birch pulps as revealed by solid-state NMR spectroscopic methods. *Cellulose* 10:307–316. <https://doi.org/10.1023/A:1027302526861>
- Ling Z, Wang T, Makarem M, Cintrón MS, Cheng HN, Kang X, Bacher M, Potthast A, Rosenau T, King H, Delhom CD, Nam S, Edwards JV, Kim SH, Xu F, French AD (2019) Effects of ball milling on the structure of cotton cellulose. *Cellulose* 26:305–328. <https://doi.org/10.1007/s10570-018-02230-x>
- Masuda K, Kaji H, Horii F (2000) CP/MAS ^{13}C NMR analyses of hydrogen bonding and the chain conformation in the crystalline and noncrystalline regions for poly(vinyl alcohol) films. *J Polym Sci B Polym Phys* 38:1–9. <https://doi.org/10.1002/ma9801265>
- Mata TM, Martins AA, Caetano NS (2018) Bio-refinery approach for spent coffee grounds valorization. *Bioresour Technol* 247:1077–1084. <https://doi.org/10.1016/j.biortech.2017.09.106>
- Miyamoto H, Yamane C, Ueda K (2013) Structural changes in the molecular sheets along (hk0) planes derived from cellulose I_β by molecular dynamics simulations. *Cellulose* 20:1089–1098. <https://doi.org/10.1007/s10570-013-9915-5>
- Murthy PS, Naidu MM (2012) Sustainable management of coffee industry by-products and value addition—a review. *Resour Conserv Recycl* 66:45–58. <https://doi.org/10.1016/j.resconrec.2012.06.005>
- Mussatto SI, Machado EMS, Martins S, Teixeira JA (2011a) Production, composition, and application of coffee and its industrial residues. *Food Bioprocess Technol* 4:661–672. <https://doi.org/10.1007/s11947-011-0565-z>
- Mussatto SI, Carneiro LM, Silva JPA, Roberto IC, Teixeira JA (2011b) A study on chemical constituents and sugars extraction from spent coffee grounds. *Carbohydr Polym* 83:368–374. <https://doi.org/10.1016/j.carbpol.2010.07.063>
- Nishiyama Y, Langan P, Chanzy H (2002) Crystal structure and hydrogen-bonding system in cellulose I_β from synchrotron X-ray and neutron fiber diffraction. *J Am Chem Soc* 124:9074–9082. <https://doi.org/10.1021/ja0257319>
- Obruca S, Benesova P, Kucera D, Petrik S, Marova I (2015) Biotechnological conversion of spent coffee grounds into polyhydroxyalkanoates and carotenoids. *New Biotechnol* 32:569–574. <https://doi.org/10.1016/j.nbt.2015.02.008>
- Ohno T, Nishio Y (2007) Estimation of miscibility and interaction for cellulose acetate and butyrate blends with *N*-vinylpyrrolidone copolymers. *Macromol Chem Phys* 208:622–634. <https://doi.org/10.1002/macp.200600510>
- Okita Y, Saito T, Isogai A (2010) Entire surface oxidation of various cellulose microfibrils by TEMPO-mediated oxidation. *Biomacromolecules* 11:1696–1700. <https://doi.org/10.1021/bm100214b>
- Panyasiri P, Yingkamhaeng N, Lam NT, Sukyai P (2018) Extraction of cellulose nanofibrils from amylase-treated cassava bagasse using high-pressure homogenization. *Cellulose* 25:1757–1768. <https://doi.org/10.1007/s10570-018-1686-6>
- Park S, Johnson DK, Ishizawa CI, Parilla PA, Davis MF (2009) Measuring the crystallinity index of cellulose by solid state ^{13}C nuclear magnetic resonance. *Cellulose* 16:641–647. <https://doi.org/10.1007/s10570-009-9321-1>
- Park S, Baker JO, Himmel ME, Parilla PA, Johnson DK (2010) Cellulose crystallinity index: measurement techniques and their impact on interpreting cellulase performance. *Biotechnol Biofuels* 3:10. <https://doi.org/10.1186/1754-6834-3-10>
- Pelissari FM, Sobral PJA, Menegalli FC (2014) Isolation and characterization of cellulose nanofibers from banana peels. *Cellulose* 21:417–432. <https://doi.org/10.1007/s10570-013-0138-6>
- Pennells J, Godwin ID, Amiralian N, Martin DJ (2019) Trends in the production of cellulose nanofibers from non-wood sources. *Cellulose*. <https://doi.org/10.1007/s10570-019-02828-9>
- Phyo P, Wang T, Yang Y, O'Neill H, Hong M (2018) Direct determination of hydroxymethyl conformations of plant cell wall cellulose using ^1H polarization transfer solid-state NMR. *Biomacromolecules* 19:1485–1497. <https://doi.org/10.1021/acs.biomac.8b00039>
- Plaza MG, González AS, Pevida C, Pis JJ, Rubiera F (2012) Valorisation of spent coffee grounds as CO_2 adsorbents for postcombustion capture applications. *Appl Energy*

- 99:272–279. <https://doi.org/10.1016/j.apenergy.2012.05.028>
- Poletto M, Pistor V, Zattera AJ (2013) Structural characteristics and thermal properties of native cellulose. *Cellulose-Fundam Asp* 2:46–68. <https://doi.org/10.5772/50452>
- Puangsin B, Yang Q, Saito T, Isogai A (2013) Comparative characterization of TEMPO-oxidized cellulose nanofibril films prepared from non-wood resources. *Int J Biol Macromol* 59:208–213. <https://doi.org/10.1016/j.ijbiomac.2013.04.016>
- Rohaizu R, Wanrosli WD (2017) Sono-assisted TEMPO oxidation of oil palm lignocellulosic biomass for isolation of nanocrystalline cellulose. *Ultrason Sonochem* 34:631–639. <https://doi.org/10.1016/j.ultsonch.2016.06.040>
- Rongpipi S, Ye D, Gomez ED, Gomez EW (2019) Progress and opportunities in the characterization of cellulose—an important regulator of cell wall growth and mechanics. *Front Plant Sci* 9:1894. <https://doi.org/10.3389/fpls.2018.01894>
- Saito T, Shibata I, Isogai A, Suguri N, Sumikawa N (2005) Distribution of carboxylate groups introduced into cotton linters by the TEMPO-mediated oxidation. *Carbohydr Polym* 61:414–419. <https://doi.org/10.1016/j.carbpol.2005.05.014>
- Saito T, Kimura S, Nishiyama Y, Isogai A (2007) Cellulose nanofibers prepared by TEMPO-mediated oxidation of native cellulose. *Biomacromolecules* 8:2485–2491. <https://doi.org/10.1021/bm0703970>
- Scherrer P (1918) Bestimmung der Grösse und der inneren Struktur von Kolloidteilchen mittels Röntgenstrahlen. *Nachr Ges Wiss Göttingen* 26:98–100
- Shang YF, Xu JL, Lee WJ, Um BH (2017) Antioxidative polyphenolics obtained from spent coffee grounds by pressurized liquid extraction. *S Afr J Bot* 109:75–80. <https://doi.org/10.1016/j.sajb.2016.12.011>
- Vítězová M, Jančíková S, Dordević D, Vítěz T, Elbl J, Hanišáková N, Jampílek J, Kushkevych I (2019) The possibility of using spent coffee grounds to improve wastewater treatment due to respiration activity of microorganisms. *Appl Sci* 9:3155. <https://doi.org/10.3390/app9153155>
- Wang CH, Wen WC, Hsu HC, Yao BY (2016) High-capacitance KOH-activated nitrogen-containing porous carbon material from waste coffee grounds in supercapacitor. *Adv Powder Technol* 4:1387–1395. <https://doi.org/10.1016/j.apt.2016.04.033>
- Wise LE, Murphy M, D'Addieco AA (1946) Chlorite holocellulose, its fractionation and bearing on summative wood analysis and on studies on the hemicelluloses. *Pap Trade J* 122:35–43
- Yang E, Qin X, Wang S (2008) Electrospun crosslinked polyvinyl alcohol membrane. *Mater Lett* 62:3555–3557. <https://doi.org/10.1016/j.matlet.2008.03.049>
- Yang H, Wang T, Oehme D, Petridis L, Hong M, Kubicki JD (2018) Structural factors affecting ^{13}C NMR chemical shifts of cellulose: a computational study. *Cellulose* 25:23–36. <https://doi.org/10.1007/s10570-017-1549-6>

Publisher's Note Springer Nature remains neutral with regard to jurisdictional claims in published maps and institutional affiliations.